crystals

MDPI

Article

Crystal Structures of $CuCl_2 \cdot 2H_2O$ (Eriochalcite) and $NiCl_2 \cdot 6H_2O$ (Nickelbischofite) at Low Temperature: Full Refinement of Hydrogen Atoms Using Non-Spherical Atomic Scattering Factors

René T. Boeré [1,2]

[1] Department of Chemistry and Biochemistry, University of Lethbridge, Lethbridge, AB T1K 3M4, Canada; boere@uleth.ca; Tel.: +1-4033292045
[2] Canadian Centre for Research in Applied Fluorine Technologies, 4401 University Drive W., Lethbridge, AB T1K 3M4, Canada

Abstract: New structure determinations of $CuCl_2 \cdot 2H_2O$ and $NiCl_2 \cdot 6H_2O$ are reported from 100 K X-ray diffraction experiments using both Mo Kα and Cu Kα radiation. Combined density functional theory (ORCA) and non-spherical atomic scattering factor (NoSpherA2) computations enabled Hirshfeld atom refinements (HAR) using custom atom scattering factors based on accurately polarized atom electron densities. The water hydrogen atoms could be positionally refined resulting in distinctly longer O–H bond lengths than those reported from previous X-ray diffraction experiments, but in good agreement with legacy neutron diffraction studies. Anisotropic displacement factors were employed, for the first time in these compounds by any technique. The outcomes from using the different X-ray sources with this new HAR method are compared, and the precision of the H-atom refinements evaluated where possible.

Keywords: X-ray crystallography; Hirshfeld atom refinement; hydrogen bonding; hydrates

Citation: Boeré, R.T. Crystal Structures of $CuCl_2 \cdot 2H_2O$ (Eriochalcite) and $NiCl_2 \cdot 6H_2O$ (Nickelbischofite) at Low Temperature: Full Refinement of Hydrogen Atoms Using Non-Spherical Atomic Scattering Factors. *Crystals* **2023**, *13*, 293. https://doi.org/10.3390/cryst13020293

Academic Editor: Vladislav V. Gurzhiy

Received: 31 December 2022
Revised: 3 February 2023
Accepted: 5 February 2023
Published: 9 February 2023

1. Introduction

The simple salts of the transition metals and their hydrates are important in chemistry, technology, and mineralogy. They provided some of the earliest examples of "complex" ions with coordinated water ligands [1]. One of the best known is the intensely blue pentahydrate $CuSO_4 \cdot 5H_2O$, the *blue vitriol of copper*, which is better formulated as $[CuSO_4(H_2O)_4] \cdot H_2O$ to differentiate coordinated and co-crystallized water [2]. Similarly, the actual bonding in the common copper(II) chloride dihydrate (**1**, mineral form: eriochalcite [3]) and nickel(II) chloride hexahydrate (**3**, mineral form: nickelbischofite [4]), which are the focus of this paper, is not evident from their names. The relationships of the structures of the hydrates to those of the anhydrous salts $CuCl_2$ (**2**) and $NiCl_2$ (**4**) are important to their hygroscopic nature and their heats of hydration (Scheme 1).

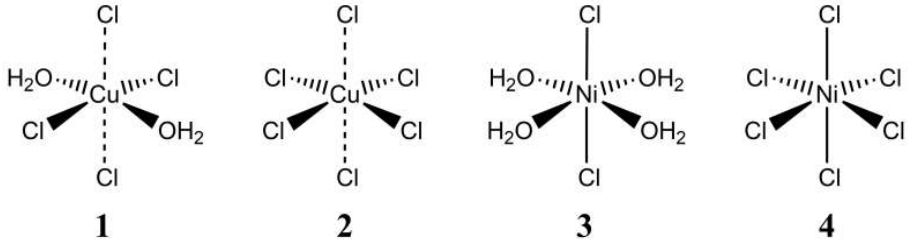

Scheme 1. Local coordination environments of the hydrated and anhydrous chlorides.

Recently, there has been a flurry of interest in metal salt hydrates for thermochemical energy storage in conjunction with the implementation of green energy sources [5,6].

Both $NiCl_2$ and $CuCl_2$ have been considered for such applications [7]. Notably, the specific crystalline forms of anhydrate and hydrate have been invoked in the evaluation of materials for such applications [8]. These hydrates are generally well known, for example, **1** is correctly described in the comprehensive textbook *Inorganic Chemistry* by Housecraft and Sharpe [9]. However, **3** is incorrectly described therein as a salt of $[Ni(OH_2)_6]^{2+}$, indicating there is an ongoing need for structural information on these foundational compounds.

Interest in the paramagnetic chlorides of Cu(II), especially **1** and **2,** remains strong. The thermal behaviour of **1** has been monitored using Raman scattering spectroscopy, whereby the transition from the orthorhombic dihydrate to the monoclinic anhydrate could be related to the vibrational modes of the two phases [10]. The magnetic properties of **1** have recently been determined and contrasted to those of the deuteride $CuCl_2{\cdot}2D_2O$ [11]. The unit cell volume in the deuterated system was found to be about 1.5% larger, implying slightly larger average separations between copper centres. The observed slightly weaker exchange interactions are consistent with the slightly smaller T_{max} and T_c in $CuCl_2{\cdot}2D_2O$. A novel 2D paramagnetic NMR technique has been applied to powdered $CuCl_2{\cdot}2D_2O$, demonstrating that the paramagnetic shift anisotropy can act as a sensitive probe of distances in paramagnetic solids [12]. Raman spectroscopy has identified librational bands due to H_2O at around 672 cm^{-1} in eriochalcite [13], in good agreement with previous work [10]. Key interest in the structures of **3** and **4** has been in relation to their antiferromagnetic structures at low temperatures [14–16]. Recent work has demonstrated that this antiferromagnetic character is preserved in nanoparticles of **4** [17]. Large single crystals of **3** are of great interest for optical UV filters, and the optical properties of such crystals have been carefully compared to those of aqueous solutions of Ni^{2+} salts [18].

Refinement with NoSpherA2. It is now recognized that improvements in crystal structure refinement models from X-ray diffraction are needed, since even routine datasets obtained on modern home-lab instruments are often of a quality that outpaces the assumptions of the independent atom method (IAM) employed as the default method in chemical and mineralogical structure determinations [19,20]. A characteristic feature of the IAM is the use of neutral atom scattering factors, which may not be appropriate in simple ionic crystal structures such as transition metal halides [21]. Another deficiency of the IAM is that H-nuclei must be placed too close to the atoms they are bonded to, whereas neutrons directly detect the nuclei and hence place them accurately in structures [22].

Fast and accurate density functional theory (DFT) methods now make it entirely feasible to compute accurate, custom, atom scattering factors that directly reflect the electron densities of atoms polarized correctly to the precise location of each atom in a structure. This approach remains a fully experimental structure determination, using the DFT to calculate custom atomic scattering factors, which are then used to refine the structure in standard applications. The method, known as Hirshfeld atom refinement (HAR) [19], has been implemented in the program NoSpherA2 [21], and incorporated into the popular structure determination package Olex2 v.1.5 [23]. HAR is undertaken with the ORCA [24] computational package in conjunction with X-ray structure refinement using olex2.refine [25], implemented with modern programming languages in an open-source, extensible environment. HAR is now becoming generally recognized as a reliable methodology to improve on IAM refinements [26], but whilst the concept that "hydrogen atoms can be located accurately and precisely by x-ray crystallography" has been endorsed [27], the uptake by chemical or mineralogical crystallographers has so far been minimal. Thus, only about 5 of the 168 citations of ref. [20] recorded in the Web of Science involve applications of the method, rather than focusing on theory or further method development. Encouragingly, some 15 of the citations of the NoSpherA2 method [21] deal primarily with applications, including some of our results [2,28,29]. Two previous applications of HAR to metal hydrates are especially relevant to this work [30,31].

Here, we report X-ray crystal structures using HAR on **1** and **3**, enabling the refinement of anisotropic displacement ellipsoids for the first time. The precision of the placement of

H-atoms is reviewed between structures determined with Cu Kα and Mo Kα sources, as well as with earlier neutron diffraction data.

2. Results and Discussion

2.1. X-Ray Diffraction Structure of $CuCl_2 \cdot 2H_2O$

The local coordination environment at Cu is shown in Figure 1. $CuCl_2 \cdot 2H_2O$, **1**, crystallizes in Pmna with the trans-disposed water molecules and the copper along a two-fold axis through the centre of the unit cell, and parallel to the *a* axis and the Cu, and four Cl ions on the mirror plane perpendicular to *a*. The primary structural data (Table 1) are in agreement with earlier X-ray [32–35] and neutron [36] diffraction data. The trans-disposed Cu–Cl1 and Cu–Cl1 ^{vi} bonds are short, 2.2870(3) Å, and along with the two water ligands form an orthogonal square planar geometry that is site-symmetry controlled. The longer, also trans-disposed Cu–Cl1 ^{ii} and Cu–Cl1 ^{v} bonds are at 2.9023(3) Å and are slightly offset from perpendicular, such that the Cl1–Cu1–Cl1 ^{v} angle is 91.10(1)°. The short–long pattern in bonds to Cl is expected for a "pseudo-Jahn-Teller" elongated d^9 electron configuration at Cu(II) [37]. The Cu1–O1 distance is 1.9420(9) Å for the coordinated aqua ligand, in excellent agreement with 1.94 Å for bonds to equatorial water oxygen atoms found by Ohtaki in aqueous Cu(II) ions from X-ray scattering probability distribution curves [38]. The axial halides belong to $CuCl_2(OH_2)_2$ moieties from the layers above and below the depicted molecule through perpendicular secondary bonding (see also Figure 2).

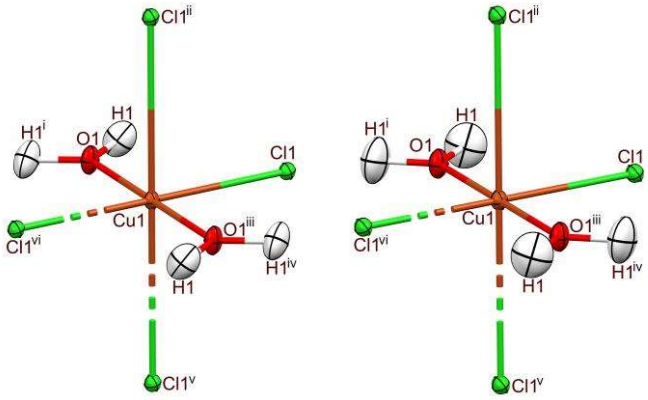

Figure 1. Displacement ellipsoids plots (40% probability) of the asymmetric units in the crystal structures of **1** determined from single crystals at 100 K, with the atom numbering schemes: (**left**) **1a** Mo Kα; (**right**) **1b** Cu Kα. Expansions to show full coordination at one Cu(II) ion (symmetry operators: *i* x,-y,1-z; *ii* x,1-y,1-z; *iii* 1-x,1-y,1-z; *iv* 1-x,y,z; *v* x,1+y,z; *vi* x,1-y,1-z).

Table 1. Selected interatomic distances (Å) and angles (°) in structures **1a** and **1b** [1].

Atoms [2]	Mo Kα–1a	Cu Kα–1b
Cu1–Cl1	2.2870(3)	2.2823(4)
Cu1–Cl1 ^{ii}	2.9023(3)	2.8973(4)
Cu1–O1	1.9420(9)	1.9414(16)
O1–H1	0.941(14)	0.95(2)
Cl1–Cu1–Cl1 ^{vi}	180.0	180.0
Cl1 ^{ii} –Cu1–Cl1^{v}	180.0	180.0
O1–Cu1–O1 ^{iii}	180.0	180.0
Cl1–Cu1–O1	90.0	90.0
Cl1–Cu1–Cl1 ^{v}	91.10(1)	91.14(1)
Cl1 ^{ii} –Cu1–O1	90.0	90.0
Cu1–O1–H1	123.7(10)	126.5(16)
H1–O1–H1 ^{i}	112.5(19)	107(3)

[1] Angles around Cu to O1 and Cl1 are symmetry controlled. [2] Sym codes: ^{i} x,-y,1-z; ^{ii} x,1-y,1-z; ^{iii} 1-x,1-y,1-z; ^{v} x,1+y,z; ^{vi} x,1-y,1-z.

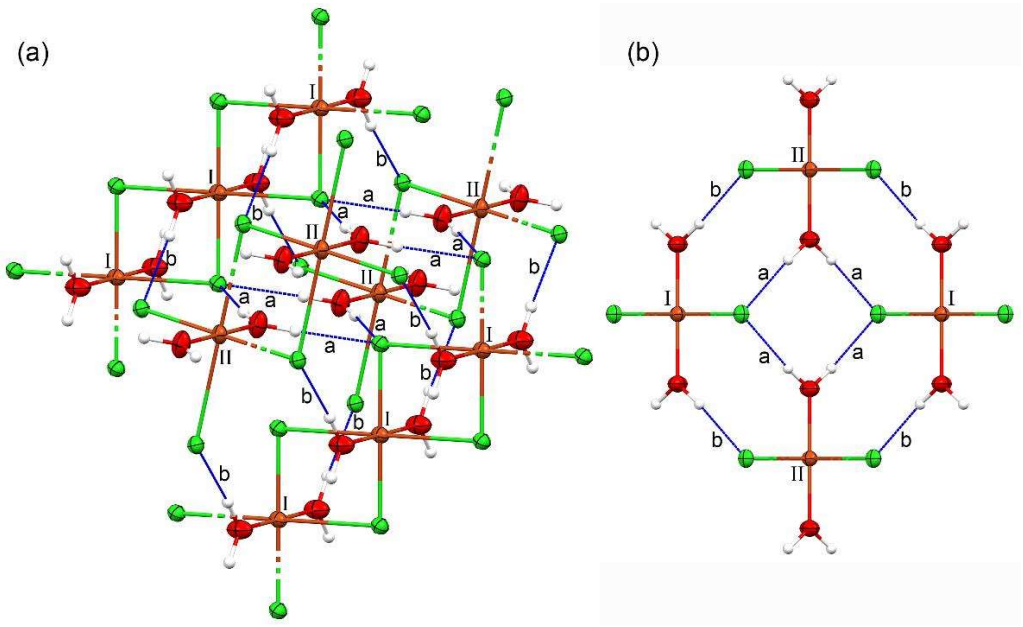

Figure 2. The lattice structure of **1** (using Cu Kα data; H-atoms drawn as spheres of 0.15 Å radius and H-bonds drawn as dashed blue lines). (**a**) Projection along the *ab* bisector showing upper, middle, and lower layers. (**b**) Projection down the *b* axis. See text for further details.

In the lattice structure of **1** (Figure 2), the layers of $CuCl_2(OH_2)_2$ contain chains linked via bridging axial contacts; parts of two such chains are shown (the three left-side and three right–side Cu atoms labeled I in Figure 2a; in projection, these are the left and right I in Figure 2b). This layer is linked by Cl···OH H-bonds to the next layers on either side (two pairs of bridged Cu atoms in these layers are labelled II in Figure 2a; in projection, the upper and lower II in Figure 2b). The "square planar" CuO_2Cl_2 moieties, involving the shorter Cu–Cl bonds in the type I and type II chains, are rotated by 77.9° from each other. The primary H-bonding contacts, ($C_1^1(4)$ chains in Etter notation [39], labelled b in the figure) always involve a type I chloro ligand acceptor and a type II water O–H donor. Larger $R_2^4(8)$ rings are defined by four such H-bonds linking two type I and two type II centres (labelled a in the figure). For alternative representations of the lattice structure of **1**, see [10].

The accurate placement of the H-atom position is of course essential for the description of the H-bond network (Table 2). The O1–H1 length determined as 0.941(14) Å from dataset **1a** in our NoSpherA2 HAR is in good agreement with the 0.95 Å from the legacy RT neutron diffraction structure [36], but all our data exceed the precision of the very limited available neutron data. By contrast, the best (RT) X-ray diffraction structure reported before this work measured this value as 0.82 Å, i.e., about 14% shorter [35]. In the direct precursor IAM refinement of this dataset (olex2.refine), this O1–H1 length is even shorter at 0.783(17) Å. Hence, a distinct advantage of HAR is this accurate placement of H-atoms, which obviates the need to artificially adjust the bonds involved in H-bonding as was previously necessary [20]. The single water molecule in **1** is coordinated to the metal and the OH_2 moiety is co-planar with equatorial $CuCl_2O_2$. This defines the O–H bond as *Class 1* according to Chiari and Ferraris [40], those for which the envelope tip angle $\varepsilon \leq 30°$. Chandler et al. using a metadata analysis (on neutron data), gave the range of such Class 1 coordinated water O–H bonds as 0.858–1.003 with a mean of 0.958 Å [41]. Our values from both datasets are very close to this mean.

Table 2. Hydrogen bonds and hydrogen displacement data for **1** and **3**.

D-H···A	d(D-H)/Å	D(H-A)/Å	d(D-A)/Å	D-H-A/°	*U*eq
1					
O1-H1···Cl1 [i a]	**0.941(14)**	**2.240(14)**	**3.1686(7)**	**169.2(14)**	**0.030(4)**
[b]	0.95(2)	2.22(2)	3.1627(11)	173(2)	0.046(7)
[c]	*0.95*	*2.24*	*3.18*	*172*	—
3					
O1-H1a···O2 [ii d]	**0.965(15)**	**1.783(14)**	**2.7401(8)**	**170.5(15)**	**0.030(4)**
[e]	0.94(3)	1.81(3)	2.7395(16)	168(3)	0.029(7)
[f]	*0.94(2)*	*1.80(2)*	*2.74(1)*	*174(2)*	*0.044(4)*
[g]	***0.96***	***1.77***	***2.73***	***170.5***	***0.027(1)***
O1-H1b···Cl [iii d]	**0.953(14)**	**2.288(15)**	**3.2049(6)**	**161.3(13)**	**0.035(45)**
[e]	0.94(3)	2.32(3)	3.2013(12)	155(2)	0.029(7)
[f]	*0.94(2)*	*2.30(2)*	*3.21(1)*	*164(2)*	*0.043(4)*
[g]	***0.97***	***2.26***	***3.19***	***161.8***	***0.029(1)***
O2-H2a···Cl [iv d]	**0.957(19)**	**2.209(19)**	**3.1420(10)**	**164.7(18)**	**0.029(5)**
[e]	1.01(5)	2.13(5)	3.1368(18)	175(4)	0.035(11)
[f]	*1.07(3)*	*2.11(3)*	*3.17(2)*	*165(1)*	*0.015(5)*
[g]	***0.97(1)***	***2.16(1)***	***3.109(7)***	***168(1)***	***0.022(3)***
O2-H2b···O1 [v d]	**0.91(2)**	**2.259(18)**	**3.0186(10)**	**140.2(6)**	**0.050(7)**
[e]	0.92(4)	2.25(3)	3.0176(18)	140.3(9)	0.029(10)
[f]	*0.96 (4)*	*2.27(2)*	*3.06(1)*	*138.3*	*0.075(1)*
[g]	**0.95(1)**	**2.23**	***3.007***	***138.4***	***0.025(3)***

[a] Data in bold text are from structure **1a** (Mo Kα data). [b] Data in normal text are from structure **1b** (Cu Kα data). [c] Data in italics are from the 1957 single crystal neutron structure at RT and are obtained from the archived CIF COD1008760 [36]; neither s.u. values nor U_{eq} values are reported [36]. [d] Data in bold text are from structure **3a** (Mo Kα data). [e] Data in normal text are from structure **3b** (Cu Kα data). [f] Data in italics are from the 1969 single crystal neutron structure at RT and obtained from the archived CIF COD9012473 [14]. [g] Data in italic bold text are from the 1969 single crystal neutron structure at 4.2 K and obtained from the archived CIF COD90124734. Limited s.u. are available for this dataset due to restrictions imposed on the experiment by the cryostat; see the original article [14]. (Symmetry operators: [i] 1/2-*x*,+*y*,3/2-*z*; [ii] 3/2-*x*,1/2+*y*,1/2-*z*; [iii] 1/2+*x*,1/2+*y*,1/2+*z*; [iv] 1+*x*,+*y*,+*z*; [v] +*x*,1-*y*,+*z*).

Comparing structure models **1a** and **1b** shows that the s.u. of the derived parameters are ~40% higher in the latter. Thus, the Mo Kα data do give both an overall better structure (Table 1) and more precise H-atom determinations (Table 2). Looking ahead to **3a** and **3b**, the s.u. of the latter is 50% larger. Hence, the evidence is that Mo Kα is superior for XRD data modelled using HAR for metal hydrates.

2.2. Comparison to Structure of Anhydrous $CuCl_2$

The relationship between the structures of **1** and anhydrous **2**, the mineral known as tolbachite [42], is important for understanding the dynamics of the hydration/dehydration cycles involved in using the salt as a proposed thermal energy storage system [7,8]. Tolbachite, a distorted form of the cadmium iodide lattice type (Figure 3a), crystallizes in *C*2/*c*, and is centered only on a two-fold axis. It has four equatorial Cu–Cl bond distances, 2.263(6) Å, and two much longer apical Cu–Cl bond distances, 2.991(6) Å, as determined from an RT X-ray diffraction structure determination [39]. The trans-angles are exactly linear, but the cis angles are 92.4(2) and 93.6(2)°. The formation of the hydrate (Figure 3b) can be understood as the insertion of water into two of the four short Cu–Cl bonds, leading both to thermodynamically stronger Cu-O bonds and to a more robust, more elastic lattice, induced by the H-bonds from the water donors to the chloro acceptors that link chains in the offset $\{CuCl_2\}_\infty$ layers. Within layers, the equivalent Cl–Cu–Cl bridging bonds transform into the long–short alternation from the *pseudo*-Jahn-Teller distortions [37]. The mineral forms of both copper chlorides are extremely rare [42]. We are grateful for the access provided to the legacy crystal data for both X-ray and neutron diffraction by the Crystallographic Open Database (http://www.crystallography.net/cod/ accessed on 30 January 2023) [43].

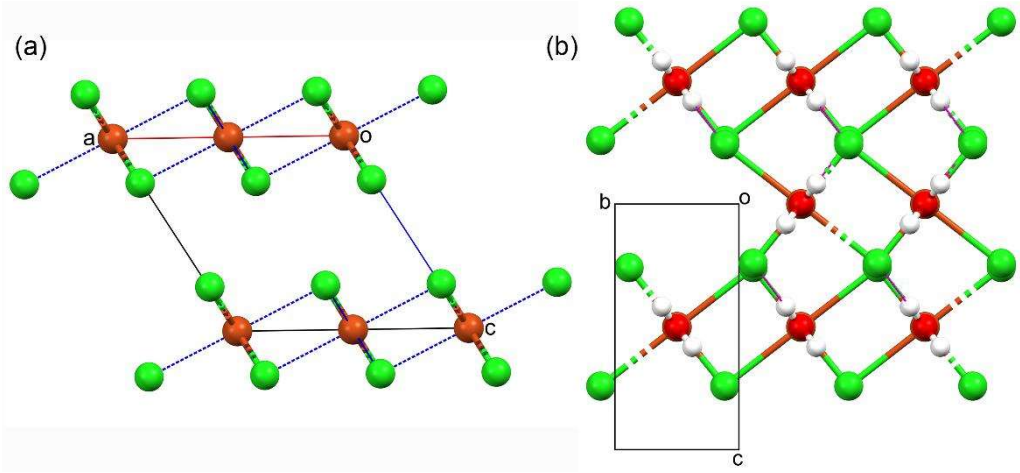

Figure 3. Comparative "ball & stick" plots of the lattice structures of (**a**) **2** and (**b**) **1** drawn to scale. Projection down the *b* axis for **2** and down the *a* axis for **1**, with each Cu centre six coordinates; unit cell boundaries for each are included. (The archival CIF COD9001506 is the source of **2** [42]).

2.3. X-ray Diffraction Structure of $NiCl_2{\cdot}6H_2O$

The local coordination environment at Ni is shown in Figure 4. $NiCl_2{\cdot}6H_2O$, **3**, crystallizes in $I2/m$ with $Z' = 0.25$, a mirror bisecting the $NiCl_2$ and $O(2)H_2$ non-coordinated water as well as $\bar{1}$ symmetry at the Ni. The trans-disposed Cu–Cl and Cu–Cl ^{i} bonds are relatively short at 2.3949(3) Å (Table 3), and along with the four symmetry-equivalent water ligands $O(1)H_2$ form a square planar coordination environment to give an overall close-to-ideal tetragonal coordination at this d^8 Ni^{2+}, affording a salt hydrate which is known to be paramagnetic [15,16]. The Ni–O distances are slightly longer than the 2.04 Å measured by Ohtaki from X-ray scattering experiments on aqueous solutions of Ni(II) ions [38]. The geometry of the Mo Kα structure determination is more precise than that obtained with copper.

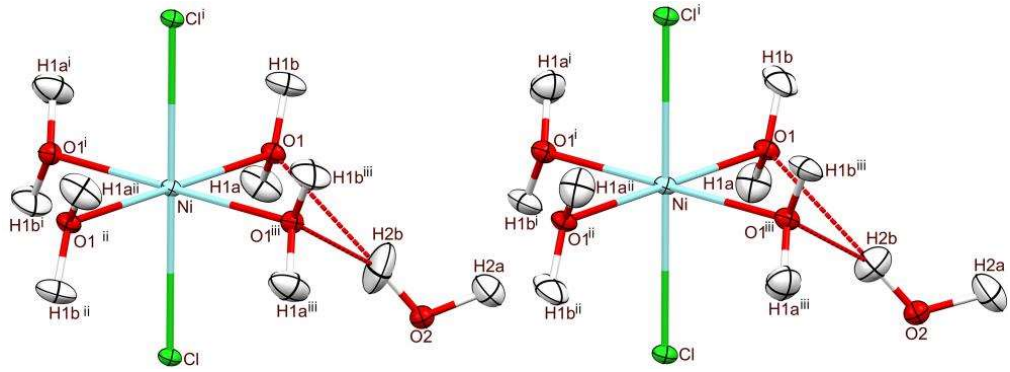

Figure 4. Displacement ellipsoids plots (50% probability) of the asymmetric units in the crystal structures of **3** determined from a single crystal at 100 K, with the atom numbering schemes: (**left**) **3a** Mo Kα; (**right**) **3b** Cu Kα. Expansions to show full coordination at one Ni(II) ion (symmetry operators: ^{i} 1-x, y,1-z; ^{ii} 1-x,1-y,1-z; ^{iii} x,1-y,z).

There is a more complex H-bonding network in the lattice of **3** than found in **1** (Figure 5), as expected with the larger number of water molecules. It should be emphasized that the nominal count of *six* water molecules from the empirical formula consists of just these two *kinds* of water, one coordinated and one only H-bonded, in a 2:1 ratio. Consequently, there are just four unique H-bond types (Table 2).

Table 3. Selected interatomic distances (Å) and angles (°) in structures **3a** and **3b** [1].

Atoms [2]	Mo Kα–3a	Cu Kα–3b
Ni–Cl	2.3949(3)	2.3936(5)
Ni–O1	2.0681(5)	2.0670(11)
O1–H1a	0.965(15)	0.94(3)
O1–H1b	0.953(14)	0.94(3)
O2–H2a	0.957(19)	1.01(5)
O2–H2b	0.91(2)	0.92(4)
Cl–Ni–Cl ^{i}	180.0	180.0
O1–Ni–O1 ^{ii}	180.0	180.0
O1 ^{i}–Ni–O1 ^{iii}	180.0	180.0
Cl–Ni–O1	89.137(17)	89.17(3)
Cl–Ni–O1 ^{ii}	90.863(17)	90.83(3)
O1–Ni–O1 ^{i}	93.19(3)	93.14(6)
O1–Ni–O1 ^{iii}	86.81(3)	86.86(6)
Ni–O1–H1a	115.2(8)	115.0(17))
Ni–O1–H1b	117.4(10)	113.1(18)
H1a–O1–H1b	106.9(13)	114(2)
H2a–O2–H2b	108(2)	115(4)

[1] Angles around Ni to O1 and Cl are symmetry controlled. [2] Sym codes: ^{i} 1-x, y,1-z; ^{ii} 1-x,1-y,1-z; ^{iii} x,1-y,z.

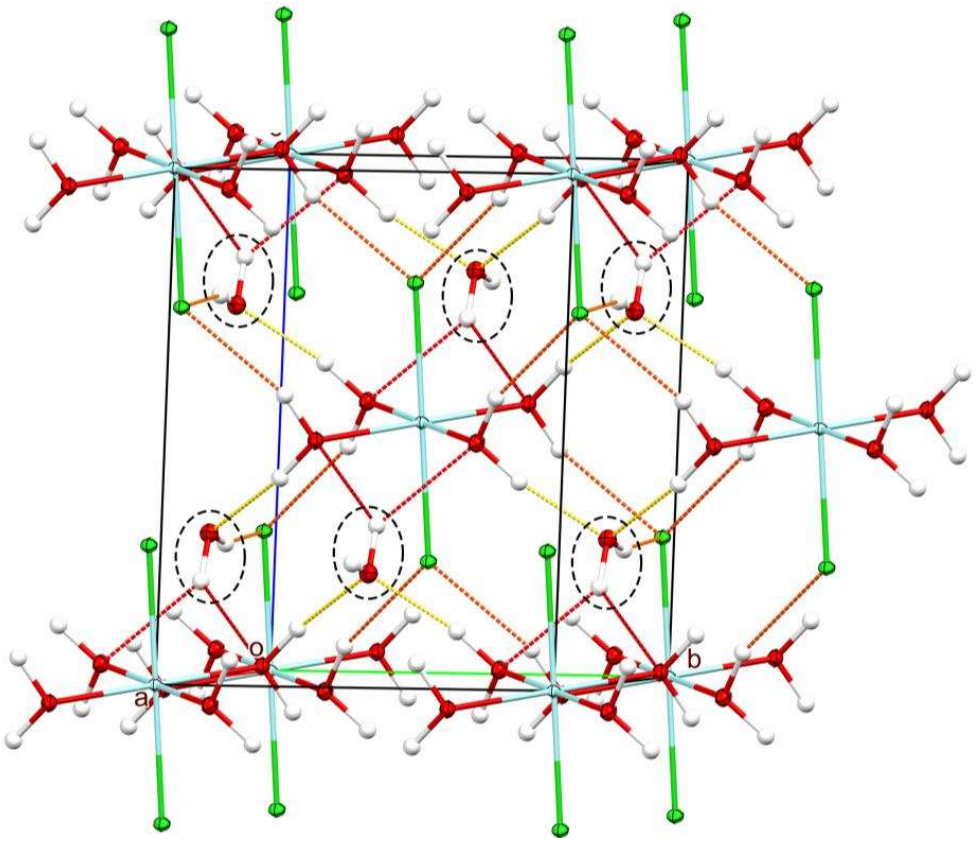

Figure 5. The lattice structure of **3** (using Mo Kα data; H-atoms drawn as spheres of 0.15 Å radius and H-bonds drawn as dashed lines that are colour-coded to relative length: yellow < orange < red). Six uncoordinated O(2)H_2 water molecules are circled for ease of identification. The two located furthest right show all H-bonds; two strong bonds as acceptors from coordinated O(1)H_2, weaker bifurcated donation to two different O1, and a single intermediate donation to Cl1. Each coordinated water donates to Cl1 and to O2 and accepts from a different O2 water. See text for further details.

The coordinated water molecule in **3**, O(1)H_2, belongs to Class 1′ according to Chiari and Ferraris, since the envelope tip angle ε in this structure is 44.1°, exceeding the limit

of 30° [40]. In the metadata analysis of Chandler et al. [41], Class 1′ coordinated water O–H bonds range from 0.917 to 1.019 with a mean of 0.972 Å (neutron data). Notably, both O1-H1A and O1-H1B lengths, 0.965(15) and 0.953(14) Å from dataset **3a**, fit comfortably within this range and are statistically indistinguishable from the mean value at the 99% confidence limit. They also fit the trend of longer bonds compared to structure **1a**, fitting the pattern from Chandler's analysis that Class 1′ > Class 1. However, very large datasets are essential to establish patterns with such small differences in the core data. By contrast, in the direct precursor IAM refinement of this X-ray dataset (olex2.refine), the four O–H lengths ranged from 0.808(11) to 0.851(13) Å, again showing the impact of the HAR.

2.4. Comparison to Structure of Anhydrous $NiCl_2$

In the structure of anhydrous $NiCl_2$, **4** (Figure 6a), each Ni atom is octahedrally coordinated by chloro ligands, but the latter each have three short bonds to Ni. These also interact with Cl atoms on neighbouring layers via contacts that exceed the sum of the v.d.W. radii by 0.18 Å [44]. In the hydrate (Figure 6b), all but two of the Ni–Cl bonds are replaced by thermodynamically stronger Ni–O bonds, and *all* the lattice-binding interactions are formed by the network of O–H···O and O–H···Cl hydrogen bonds (Table 2), producing a robust 3D lattice, in place of the layer structure, that is also much more elastic. These structural changes are relevant to use in proposed thermal energy storage systems [7,8].

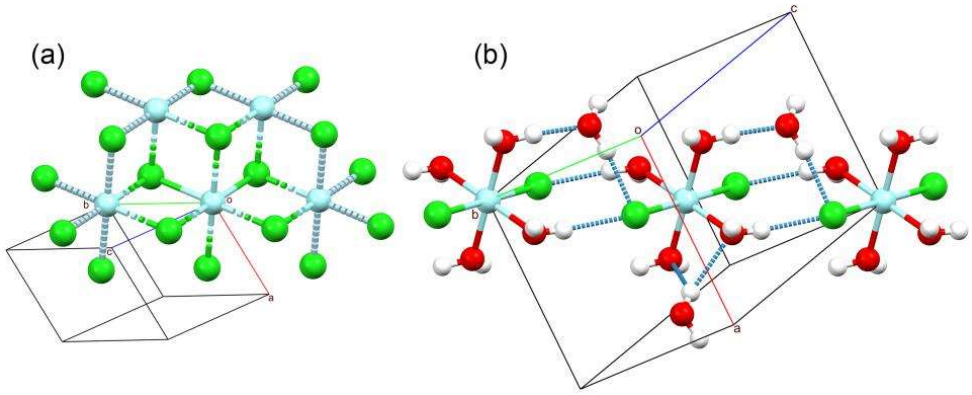

Figure 6. Comparative "ball & stick" plots of the lattice structures of (**a**) **4** and (**b**) **3** drawn to scale. Projection parallel to the *b* axis for **4** and ~ perpendicular to the body diagonal axis for **3**; unit cell boundaries for each are included. (The archival CIF COD2310380 was employed for **4** [44]).

3. Experimental Section

3.1. Sample Sources

The copper(II) chloride hydrate ($CuCl_2{\cdot}2H_2O$) crystals **1** were either sourced from Baker (Analyzed Reagent grade) and used as received, or synthesized by adding SO_2Cl_2 (13.63 mg, 0.101 mmol) in 1 mL CH_2Cl_2 to a suspension of CuCl (10.0 mg, 0.101 mmol) in 1 mL CH_2Cl_2 at 0 °C. The mixture was allowed to warm to room temperature and stirred for 30 min to complete the reaction. The solvent was evaporated, and the solid residues were dissolved in CH_3CN. Small greenish-blue crystals of $CuCl_2{\cdot}2H_2O$ were grown by slow evaporation at room temperature and were identified by X-ray diffraction. Data obtained on these synthetic crystals were overall slightly superior to crystals taken from the bulk commercial salt.

The pale-green nickel(II) chloride hydrate crystals ($NiCl_2{\cdot}6H_2O$) **3** were obtained by recrystallization of commercial salt (BDH Reagents) by cooling warmed solutions in deionized H_2O. Suitable, small, and well-formed crystals of both compounds were selected under the microscope and frozen in Paratone™ oil on 50 μm MiTeGen micromounts with the diffractometer Oxford Cryostream 800 device.

3.2. Crystallography

Data collection employed a Rigaku-Oxford Diffraction SuperNova dual microsource kappa diffractometer equipped with a Pilatus 200K HPC detector. Data collection, reduction, and correction were controlled using CrysAlisPro 1.171.42.63a (Rigaku Oxford Diffraction, 2022). Empirical absorption corrections were applied using spherical harmonics implemented in the SCALE3 ABSPACK scaling algorithm. The refinement employed NoSpherA2 [21], (NOn-SPHERical Atom-form-factors in Olex2) [23], an implementation of Hirshfeld atom refinement (HAR) that makes use of tailor-made aspherical atomic form factors calculated on-the-fly from a Hirshfeld-partitioned electron density (ED). The ED was calculated from a Gaussian basis set single determinant SCF wavefunction in DFT at the PBE/def2-TZVPP level of theory for a fragment of the crystal and a multiplicity of 2 for Cu d^9 and 3 for Ni d^8. The ORCA 5.0 software suite was employed on an i7-8700 CPU @ 3.20 GHz computer with 16.0 Gb RAM under Windows 10 [24]. NoSpherA2 was set for high accuracy partitioning. The crystal and structure refinement data are summarized in Table 4. Selected interatomic distances and angles for **1** are provided in Table 1 and for **3** in Table 3, and H-bonding data in Table 2. CheckCIF reports and data in CIF format are also available from the Supplementary Materials.

Table 4. Crystal and structure refinement data.

Parameter	1a	1b	3a	3b
Empirical formula	$Cl_2CuH_4O_2$	$Cl_2CuH_4O_2$	$Cl_2H_{12}NiO_6$	$Cl_2H_{12}NiO_6$
Formula weight	170.481	170.481	237.690	237.690
Temperature/K	100.01(10)	100.01(10)	99.98(10)	99.99(10)
Crystal system	orthorhombic	orthorhombic	monoclinic	monoclinic
Space group	*Pmna*	*Pmna*	*I*2/*m*	*I*2/*m*
a/Å	8.0553(3)	8.0405(4)	6.5628(4)	6.5579(2)
b/Å	3.7295(2)	3.7238(2)	7.0330(4)	7.0244(3)
c/Å	7.3674(3)	7.3585(4)	8.7326(6)	8.7291(3)
β/°	90	90	96.723(6)	96.702(4)
Volume/Å^3	221.333(17)	220.32(2)	400.29(4)	399.36(3)
Z, Z′	2, 0.25	2, 0.25	2, 0.25	2, 0.25
ρ_{calc}/g/cm^3	2.558	2.570	1.972	1.977
μ/mm^{-1}	5.967	16.849	3.062	9.551
F(000)	166.0	166.0	244.0	244.0
Crystal size/mm^3	0.21 × 0.04 × 0.02	0.16 × 0.07 × 0.06	0.18 × 0.1 × 0.03	0.23 × 0.09 × 0.04
Radiation	Mo Kα (λ = 0.71073)	Cu Kα (λ = 1.54184)	Mo Kα (λ = 0.71073)	Cu Kα (λ = 1.54184)
2Θ range data collect/°	7.5 to 68.94	16.32 to 149.94	7.36 to 71.44	16.04 to 160.34
Index ranges	$-13 \le h \le 13$ $-6 \le k \le 6$ $-12 \le l \le 12$	$-9 \le h \le 9$ $-4 \le k \le 4$ $-8 \le l \le 9$	$-10 \le h \le 9$ $-11 \le k \le 11$ $-14 \le l \le 13$	$-8 \le h \le 6$ $-8 \le k \le 8$ $-10 \le l \le 11$
Reflections collected	20107	1200	4133	2052
Independent reflections	499	238	890	469
R_{int}, R_{sigma}	0.0598, 0.0170	0.0186, 0.0108	0.0318, 0.0233	0.0364, 0.0227
Data/restraints/param	499/6/25	238/0/26	890/0/56	469/24/56
Goodness-of-fit on F^2	1.016	1.053	0.996	1.044
Final R indexes [$I \ge 2\sigma(I)$]	R_1 = 0.0120, wR_2 = 0.0257	R_1 = 0.0133, wR_2 = 0.0329	R_1 = 0.0175, wR_2 = 0.0396	R_1 = 0.0276, wR_2 = 0.0823
Final R indexes [all data]	R_1 = 0.0134, wR_2 = 0.0264	R_1 = 0.0133, wR_2 = 0.0329	R_1 = 0.0186, wR_2 = 0.0400	R_1 = 0.0295, wR_2 = 0.0843
Largest diff. peak/hole/e Å^{-3}	0.56/−0.42	0.26/−0.21	0.40/−0.50	0.46/−0.50
Accession codes (CCDC)	2238551	2233706	2238552	2238553

The following is a description of the operational strategy that was used in performing HAR with NoSpherA2 in this work. Of key importance is the integration of this method in the highly popular crystallographic graphical user interface (GUI) known as Olex2. The brief outline provided here should be used in conjunction with the theory provided in

references [19] and [21]. Potential adopters of the method should certainly consult the excellent on-line documentation provided by the OlexSys organization (https://www.olexsys.org/ accessed on 30 January 2023) and many extremely useful videos on the Olex2 YouTube channel (https://www.youtube.com/channel/UCV6B2W8zlmXqkU2DbIviQow accessed on 30 January 2023). NoSpherA2 operates only in conjunction with the olex2.refine engine (i.e., not with ShelXL, though the input and most instructions from the ShelXL environment work seamlessly) [25]. However, only olex2.refine has the underlying software architecture able to input the custom form factors computed by NoSpherA2. In our group, we have learned that a full refinement to publishable standards should be undertaken with the IAM first using olex2.refine, which we archived in a separate folder. We used these archives to allow for comparisons in structure precision between the IAM and HAR models. We have discovered, particularly with organic compounds, an overall improvement in structure precision with NoSpherA2 that can approach 80% for high quality datasets [28,29]. Even for inorganics, there can be a measurable improvement where adequate markers are present (e.g., multiple S–O bonds [2]). A feature of implementing NoSpherA2 is that atom labels cannot be changed after the computational process starts, and so the IAM file also provides a "backup file", from which the HAR must be restarted if significant changes to the model are later found to be necessary. Trying to make label or model changes to an active NoSpherA2 refinement model is not recommended.

A key innovation of NoSpherA2 in Olex2 is that the expanded structure required for a viable density functional theory (DFT) calculation can be arranged by symmetry and contact expansion in the GUI workspace. Very simply, whatever atoms are on the screen are computed. Thus, for **1**, the full $CuCl_2(OH_2)_2$ formula unit was used for the calculation (it would equally be possible to include the additional axial chlorides and compute $[CuCl_4(OH_2)_2]^{2-}$). Next, the appropriate charge and multiplicity for the computed entity must be assigned; therefore, for **2**, the doublet state for the d^9 electron configuration was employed. Similarly, for **3**, $[NiCl_2(OH_4)_4]\cdot H_2O$ was the computed entity (exactly as displayed in Figure 4a), and a multiplicity of 3 for the expected paramagnetic d^8 electron configuration was selected. In practice, several combinations of the structure entity should be investigated to ensure that the DFT SCF calculation is able to model the atom electron densities sufficiently accurately to allow for optimal subsequent form factor calculations (such parallel models are best stored in separate working folders). In the work reported here, the ORCA 5.0 computational method was employed because we have found it to be reliable, and above all, very fast. The SCF calculations themselves took about 9 s in the case of **1a** and a little over 4 s for **3a**. The full combination of the final iterative sequence of ORCA DFT, NoSpherA2 form factor, and olex2.refine cycles were tracked with a stopwatch and amounted to about one minute for **1a** and 1.5 min for **3a** on the standard desktop PC described above. Larger molecules obviously took longer, and total computing times exceeding 20 min were encountered for some ~150 atom molecules studied in an earlier project, albeit using an older (slower) implementation of ORCA [29].

4. Conclusions

HAR using NoSpherA2 was undertaken for $CuCl_2\cdot 2H_2O$, **1**, and $NiCl_2\cdot 6H_2O$, **3**, from dual-wavelength single-crystal X-ray diffraction experiments. The obtained O–H lengths are indistinguishable from the legacy neutron diffraction structure determinations of these common metal salt hydrates. This report provides the first crystallographic models for **1** and **3**, supposedly well-known structures, in which the hydrogen displacements ellipsoids have been fully refined. The very old and experimentally limited extant neutron refinements did not achieve this. Yet, notably, these neutron data have been used in extensive metadata analyses [41]. Therefore, there is an obvious need to revisit the structures of many of the crystalline hydrates of metal salts. Prospects for accurate H-atom placements in such salts by HAR with NoSpherA2 are extremely promising, at a modest experimental cost, and all who have access to good quality crystals, or have existing SC-XRD datasets on hand, are encouraged to apply this excellent, user-friendly method.

Supplementary Materials: The following supporting information can be downloaded at: https://www.mdpi.com/article/10.3390/cryst13020293/s1, Crystal Structure Reports for **1** and **3**; structures in CIF format.

Funding: This research received no external funding.

Data Availability Statement: CSD 2233706; 2238551-2238553 contain the supplementary crystallographic data for this paper. These data can be obtained free of charge via www.ccdc.cam.ac.uk/data_request/cif, or by emailing data_request@ccdc.cam.ac.uk, or by contacting The Cambridge Crystallographic Data Centre, 12 Union Road, Cambridge CB2 1EZ, UK; fax: +44-1223-336033 or from the Inorganic Crystal Structure Database, https://icsd.products.fiz-karlsruhe.de/ accessed on 28 January 2023.

Acknowledgments: M. A. Ibrahim prepared the synthetic sample of **1**. The support of the University of Lethbridge for the experimental work and manuscript preparation is gratefully acknowledged. The university and the Faculty of Arts and Science for providing X-ray diffraction equipment is acknowledged. The anonymous referees of this article are thanked for their constructive advice that led to strengthening the content and arguments of the paper. Remaining errors are solely the author's responsibility.

Conflicts of Interest: The author declares no conflict of interest.

References

1. Kauffman, G.B. (Ed.) *Coordination Chemistry: A Century of Progress*; Oxford University Press: Oxford, UK, 1994.
2. Ibrahim, M.A.; Boeré, R.T. The copper sulfate hydration cycle. Crystal structures of $CuSO_4$ (Chalcocyanite), $CuSO_4{\cdot}H_2O$ (Poitevinite), $CuSO_4{\cdot}3H_2O$ (Bonattite) and $CuSO_4{\cdot}5H_2O$ (Chalcanthite) at low temperature using non-spherical atomic scattering factors. *New J. Chem.* **2022**, *46*, 5479–5488. [CrossRef]
3. Scacchi, A. Dell'eriocalco e del melanotallo, nuove specie di minerali. *Rend. Dell'accademia Delle Sci. Fis. E Mat. Sez. Della Soc. R. Di Napoli* **1870**, *9*, 86–89.
4. Crook, W.W., III; Jambor, J.L. Nickelbischofite, a new nickel chloride hydrate. *Can. Mineral.* **1979**, *17*, 107–109.
5. N'Tsoukpoe, K.E.; Schmidt, T.; Rammelberg, H.U.; Watts, B.A.; Ruck, W.K.L. A systematic multi-step screening of numerous salt hydrates for low temperature thermochemical energy storage. *Appl. Energy* **2014**, *124*, 1–16. [CrossRef]
6. Glasser, L. Thermodynamics of Inorganic Hydration and of Humidity Control, with an Extensive Database of Salt Hydrate Pairs. *J. Chem. Eng. Data* **2014**, *59*, 526–530. [CrossRef]
7. Donkers, P.A.J.; Sögütoglu, L.C.; Huinink, H.P.; Fischer, H.R.; Adan, O.C.G. A review of salt hydrates for seasonal heat storage in domestic applications. *Appl. Energy* **2017**, *199*, 45–68. [CrossRef]
8. Kiyabu, S.; Girard, P.; Siegel, D.J. Discovery of Salt Hydrates for Thermal Energy Storage. *J. Am. Chem. Soc.* **2022**, *144*, 21617–21627. [CrossRef]
9. Housecroft, C.E.; Sharpe, A.G. *Inorganic Chemistry*, 4th ed.; Pearson: Harlow, UK, 2012; pp. 761–766.
10. Medeiros, F.E.O.; Araujo, B.S.; Ayala, A.P. Raman spectroscopy investigation of the thermal stability of the multiferroic $CuCl_2$ and its hydrated form. *Vib. Spectr.* **2018**, *99*, 1–6. [CrossRef]
11. DeFotis, G.C.; Hampton, A.S.; Van Dongen, M.J.; Komatsu, C.H.; Benday, N.S.; Davis, C.M.; Hays, K.; Wagner, M.J. Magnetism of $CuCl_2{\cdot}2D_2O$ and $CuCl_2{\cdot}2H_2O$, and of CuBr2·6H_2O. *J. Magn. Magn. Mater.* **2017**, *434*, 23–29. [CrossRef]
12. Antonijevic, S.; Persson, E. Study of water dynamics and distances in paramagnetic solids by variable-temperature two-dimensional 2H NMR sectroscopy. *J. Chem. Phys.* **2007**, *126*, 014504. [CrossRef]
13. Frost, R.L.; Williams, P.A.; Kloprogge, J.T.; Martens, W. Raman spectroscopy of the copper chloride minerals nantokite, eriochalcite and claringbullite—Implications for copper corrosion. *Neues Jahrb. Mineral. Monats.* **2003**, *2003*, 433–445. [CrossRef]
14. Kleinberg, R. Crystal Structure of $NiCl_2{\cdot}6H_2O$ at Room Temperature and 4.2°K by Neutron Diffraction. *J. Chem. Phys.* **1969**, *50*, 4690–4696. [CrossRef]
15. Kleinberg, R. Magnetic Structure of $NiCl_2{\cdot}6H_2O$. *J. Appl. Phys.* **1967**, *38*, 1453–1454. [CrossRef]
16. Spence, R.D.; Middents, P.; ElSaffar, Z.; Kleinberg, R. A Proton Resonance Study of the Magnetic Structure of Antiferromagnetic $CoCl_2{\cdot}6H_2O$, $CoBr_2{\cdot}6H_20$, $NiCl_2{\cdot}6H_2O$, and $NiBr_2{\cdot}6H_2O$. *J. Appl. Phys.* **1964**, *35*, 854–855. [CrossRef]
17. Enyashin, A.N.; Ivanovskii, A.L. Magnetic properties of $NiCl_2$ nanostructures. *Comput. Mater. Sci.* **2010**, *49*, 782–786. [CrossRef]
18. Zajnullin, O.B.; Voloshin, A.E.; Komornikov, V.A.; Manomenova, V.L.; Rudneva, E.B.; Timakov, I.S.; Kovalev, S.I. Some Properties of $NiCl_2{\cdot}6H_2O$ Single Crystals. *Phys. Sol. State* **2019**, *61*, 2415–2417. [CrossRef]
19. Capelli, S.C.; Burgi, H.B.; Dittrich, B.; Grabowsky, S.; Jayatilaka, D. Hirshfeld atom refinement. *IUCrJ* **2014**, *1*, 361–379. [CrossRef]
20. Woińska, M.; Grabowsky, S.; Dominiak, P.M.; Woźniak, K.; Jayatilaka, D. Hydrogen atoms can be located accurately and precisely by x-ray crystallography. *Sci. Adv.* **2016**, *2*, e1600192. [CrossRef]

21. Kleemiss, F.; Dolomanov, O.V.; Bodensteiner, M.; Peyerimhoff, N.; Midgley, L.; Bourhis, L.J.; Genoni, A.; Malaspina, L.A.; Jayatilaka, D.; Spencer, J.L.; et al. Accurate crystal structures and chemical properties from NoSpherA2. *Chem. Sci.* **2021**, *12*, 1675–1692. [CrossRef]
22. Bacon, G.E. *Neutron Diffraction*, 3rd ed.; Clarendon Press: Oxford, UK, 1975.
23. Dolomanov, O.V.; Bourhis, L.J.; Gildea, R.J.; Howard, J.A.K.; Puschmann, H. OLEX2: A complete structure solution, refinement and analysis program. *J. Appl. Crystallogr.* **2009**, *42*, 339–341. [CrossRef]
24. Neese, F. Software update: The ORCA program system Version 5.0. *WIREs Comput. Mol. Sci.* **2022**, *12*, e1606. [CrossRef]
25. Bourhis, L.J.; Dolomanov, O.V.; Gildea, R.J.; Howard, J.A.; Puschmann, H. The anatomy of a comprehensive constrained, restrained refinement program for the modern computing environment—Olex2 dissected. *Acta Crystallogr. Sect. A* **2015**, *71*, 59–75. [CrossRef] [PubMed]
26. Cooper, R.I. Recent developments in the refinement and analysis of crystal structures. *Struct. Bond.* **2020**, *185*, 43–68. [CrossRef]
27. Farrugia, L.J. Accurate H-atom parameters from X-ray diffraction data. *IUCrJ* **2014**, *1*, 265–266. [CrossRef]
28. Hill, N.D.D.; Lilienthal, E.; Bender, C.O.; Boeré, R.T. Accurate crystal structures of C12H9CN, C12H8(CN)2, and C16H11CN valence isomers using nonspherical atomic scattering factors. *J. Org. Chem.* **2022**, *87*, 16213–16229. [CrossRef]
29. Marszaukowski, F.; Boeré, R.T.; Wohnrath, K. Frustrated and realized hydrogen bonding in 4-hydroxy-3,5-di*tert*butylphenylphosphine derivatives. *Cryst. Growth Des.* **2022**, *22*, 2512–2533. [CrossRef]
30. Chocolatl Torres, M.; Bernès, S.; Kuri, U.S. Refinement of $K[HgI_3]\cdot H_2O$ using non-spherical atomic form factors. *Acta Crystallogr.* **2021**, *E77*, 681–685. [CrossRef]
31. Chrappová, J.; Pateda, Y.R.; Rakovský, E. Synthesis and Crystal Structure Analysis of $NH_4[Zn(cma)(H_2O)_2]\cdot H_2O$ Using IAM and HAR Approaches. *J. Chem. Crystallogr.* **2022**. [CrossRef]
32. Harker, D. The Crystal Structure of Cupric Chloride Dihydrate $CuCl_2\cdot 2H_2O$. *Z. Kristallogr.* **1936**, *93*, 136–145. [CrossRef]
33. MacGillavry, C.H.; Bijvoet, J.M. Die Kristallstruktur der Cadmium- und Quecksilber-Diamin-Dihalogenide. *Z. Kristallogr.* **1936**, *94*, 231–245. [CrossRef]
34. Engberg, A. An X-ray refinement of the crystal structure of copper(II) chloride dihydrate. *Acta Chem. Scand.* **1970**, *24*, 3510–3526. [CrossRef]
35. Brownstein, S.; Han, N.F.; Gabe, E.; LePage, Y. A redetermination of the crystal structure of cupric chloride dihydrate. *Z. Kristallogr.* **1989**, *189*, 13–15. [CrossRef]
36. Peterson, S.W.; Levy, H.A. Proton Positions in $CuCl_2\cdot 2H_2O$ by Neutron Diffraction. *J. Chem. Phys.* **1957**, *26*, 220. [CrossRef]
37. Halcrow, M.A. Jahn-Teller distortions in transition metal compounds, and their importance in functional molecular and inorganic materials. *Chem. Soc. Rev.* **2013**, *42*, 1784–1795. [CrossRef]
38. Ohtaki, H.; Yamaguchi, T.; Maeda, M. X-ray diffraction studies of the structures of hydrated divalent transition-metal ions in aqueous solution. *Bull. Chem. Soc. Jpn.* **1976**, *49*, 701–708. [CrossRef]
39. Etter, M.C. Encoding and decoding hydrogen-bond patterns of organic compounds. *Acc. Chem. Res.* **1990**, *23*, 120–126. [CrossRef]
40. Chiari, G.; Ferraris, G. The water molecule in crystalline hydrates studied by neutron diffraction. *Acta Crystallogr. Sect. B Struct. Crystallogr. Cryst. Chem.* **1982**, *38*, 2331–2341. [CrossRef]
41. Chandler, G.S.; Wajrak, M.; Khan, R.N. Neutron diffraction structures of water in crystalline hydrates of metal salts. *Acta Crystallogr. B Struct. Sci. Cryst. Eng. Mater.* **2015**, *71*, 275–284. [CrossRef]
42. Burns, P.C.; Hawthorne, F.C. Tolbachite, $CuCl_2$, the first example of Cu^{2+} octahedrally coordinated by Cl^-. *Am. Mineral* **1993**, *78*, 187–189.
43. Grazulis, S.; Chateigner, D.; Downs, R.T.; Yokochi, A.T.; Quiros, M.; Lutterotti, L.; Manakova, E.; Butkus, J.; Moeck, P.; Le Bail, A. Crystallography Open Database—An open-access collection of crystal structures. *J. Appl. Crystallogr.* **2009**, *42*, 726–729. [CrossRef]
44. Ferrari, A.; Braibanti, A.; Bigliardi, G. Refinement of the crystal structure of $NiCl_2$ and of unit-cell parameters of some anhydrous chorides of divalent metals. *Acta Crystallogr.* **1963**, *16*, 846–847. [CrossRef]